Nano Research

Open Access

Research Article

Strain-controlled current-induced magnetization switching in flexible spin-orbit torque device

Meiling Li[1], Xiaoguang Xu[1] ✉, Mengxi Wang[2], Bin He[3], Tanzhao Zhang[1], Jianqin Guo[1], Kangkang Meng[1], Guoqiang Yu[3], and Yong Jiang[1] ✉

[1] Key Laboratory of Advanced Materials and Devices for Post-Moore Chips, Ministry of Education, School of Materials Science and Engineering, University of Science and Technology Beijing, Beijing 100083, China
[2] Key Laboratory of Spintronics Materials, Devices and Systems of Zhejiang Province, Hangzhou 311300, China
[3] Beijing National Laboratory for Condensed Matter Physics, Institute of Physics, Chinese Academy of Sciences, Beijing 100190, China

Cite this article: *Nano Research*, **2025**, *18*, 94907066. https://doi.org/10.26599/NR.2025.94907066

ABSTRACT: Spin-orbit torque (SOT)-based flexible devices have been proved to be promising candidates for wearable technology and artificial intelligence. However, there is still a blank for the bending sensitive SOT devices, which hampers the applications of flexible spintronic devices. Here we report a bending strain-mediated perpendicular magnetic anisotropy (PMA) and current-induced magnetization switching in Kapton/polyimide/Ta/Pt/Co/Pt ferromagnetic heterostructures. The coercivity of anomalous Hall effect loop increases about 15% under a tensile strain of about 1.35%. Moreover, the critical current density (J_c) gradually decreases with increasing of the tensile strain, and the magnitude of J_c reduces about 7.6% under 1.35% tensile strain. It is notable that the Hall resistance can be reversible modulated by tensile strain. These strain sensitive behaviors can be attributed to the mechanical strain from the flexible substrates. This study paves the way for future train sensors and low energy consumption logic-in memory basing on mechanical strain.

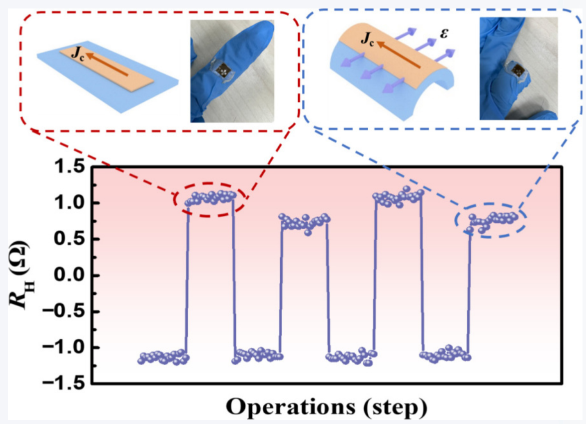

KEYWORDS: spin-orbit torque, anomalous Hall effect, flexible electronics, mechanical strain

1 Introduction

Recently, flexible spintronic devices have garnered significant attention due to their deformable and lightweight characteristics which are suitable for wearable applications [1–5]. Especially, perpendicular magnetic anisotropy (PMA) and current-induced magnetization switching via spin-orbit torques (SOT) have emerged as key topics of interest, owing to their potential applications in flexible spintronic devices [6–12]. Spintronic devices with PMA have great advantages over those with in-plane anisotropy due to their higher storage density and thermal stability [6, 13]. SOT-based magnetization switching can also be realized in the devices with PMA. SOT-based magnetic random-access memory (SOT-MRAM) has many advantages including low power dissipation and high storage density, which make it desirable for flexible applications [14–17]. To date, researchers have attempted several possibilities of integrating flexibility into ferromagnetic/heavy metal (FM/HM) systems. Researchers have put great efforts on the strain tunable magnetic properties of magnetic thin films. In 2020, Zhang et al. reported that an emergent Dzyaloshinskii-Moriya interaction can be achieved in a centrosymmetric material, $La_{0.67}Sr_{0.33}MnO_3$, by a graded strain [18]. In 2024, Jun et al. demonstrated the relationship between the strain and orbital magnetic moment in an interfacial multiferroic system with a giant magnetoelectric effect [19]. In 2021, Wen Siang Lew et al. demonstrated that the Pt/Co bilayer grown on flexible Kapton substrate showed a 45% increase of spin Hall efficiency under mechanical strain. Moreover, the enhancement can be preserved about 78% even after the strain was removed [20]. Researchers have also tried to study the SOT effect in flexible devices. In 2015, Lee et al. realized the SOT induced magnetization switching in Pt/Co/MgO heterostructure on flexible polyethylene naphthalate substrate, demonstrating the stability of the Pt/Co/MgO system

Received: August 29, 2024; **Revised:** October 9, 2024
Accepted: October 10, 2024

✉Address correspondence to Xiaoguang Xu, xgxu@ustb.edu.cn; Yong Jiang, yjiang@ustb.edu.cn

under strain [11]. According to these studies, SOT-induced magnetization switching is sensitive to the magnetization states of the FM layer which has also been demonstrated tunable by strain. Therefore, it is reasonable to expect that the SOT behaviors can be modulated by strain. In 2020, the SOT-driven magnetization switching ratio was demonstrated to be tunable by the in-plane strain on piezoelectric substrate [21]. However, the modulation on current-induced magnetization switching of flexible devices under bending strain is still in its infancy. It is necessary to reveal how the SOT behavior of flexible devices responds to bending strain state, which is crucial for strain sensors, especially in wearable applications.

In this work, we study bending tensile strain mediated PMA and SOT-based current-induced magnetization switching in Kapton/polyimide (PI)/Ta/Pt/Co/Pt multilayers. It was found that the magnetic anisotropy of the ferromagnetic layer can be controlled by the mechanical strain. Furthermore, the critical current density (J_c) of current-induced magnetization switching can also be modified by tensile strain, which performs a promotion effect of the strain on SOT behavior.

2 Results and discussion

The flexible device was schematically illustrated in Figs. 1(a)–1(c) and the stacking structure of Kapton/PI/Ta (1)/Pt (3)/Co (1.5)/Pt (1) (thickness in nm) was shown in Fig. 1(d). The surface of Kapton substrates was optimized by coating a PI layer. Since the surface of flexible substrates usually cannot satisfy the requirements of spintronic devices, the PI coated Kapton possesses the following advantages. First, bending cycle experiments show that the devices fabricated on the Kapton/PI will neither detach nor crack during the strain application process (Fig. S1 of in the Electronic Supplementary Material (ESM)). Second, the roughness of Kapton surface can be greatly decrease. As shown in Fig. 1(e), the root mean square roughness (R_q) of the Kapton substrate without a PI layer is measured to be about 0.98 nm by the atomic force microscope (AFM). After coating a thin PI layer, the R_q of the Kapton/PI film can even reach 0.56 nm, as shown in Fig. 1(f), which is comparable to most rigid substrates for spintronic devices. For spintronic devices, the contact between the function layer and the substrate greatly influences their behaviors. The large roughness of traditional flexible substrates might be the reason for the failure of the devices and their modulation. We have measured the AFM and R_H–I loop of Kapton/Ta (1 nm)/Pt (3 nm)/Co (1.5 nm)/Pt (1 nm) structure. As shown in Figs. S2 and S3 in the ESM, it can be concluded that the spin-coated PI layer is a key factor for the good device performance in this study. So, the coated PI layer is a key factor for the device performance in this study. Finally, when we use the photolithography technique to fabricate Hall bar devices as shown in Fig. 1(c), no crack appears on the surface of the substrate. The flat and bending states photographs of the flexible spintronic devices after various bending cycles are shown in Fig. 1(g), which demonstrates the excellent flexibility.

Before the study of strain-controlled magnetization switching, it is necessary to confirm the magnetic properties of the as-deposited Kapton/PI/Ta/Pt/Co/Pt heterostructure. The thickness of the magnetic layer is optimized first to ensure the strain sensitivity of the stacking structure in the following strain engineering of the flexible Hall bar devices. The typical thickness of the Co layer with strong PMA is 0.8 to 1.4 nm [22]. Therefore, the Co thickness is set to 1.0 and 1.5 nm, respectively. Figure S2 in the ESM and Fig. 2(b) show the out-of-plane and in-plane hysteresis (M–H) loops of the Kapton/PI/Ta/Pt/Co (1.0)/Pt and Kapton/PI/Ta/Pt/Co (1.5)/Pt multilayers, respectively. The difference of the out-of-plane and in-plane magnetization M–H loops clearly indicates the PMA of both samples. The effective magnetic anisotropy field (H_k) is estimated to be about 1497 and 1214 Oe for the samples with 1.0 and 1.5 nm Co layer [23, 24]. Therefore, the PMA of 1.0 nm Co layer sample is stronger than that of 1.5 nm. And the two groups of samples were prepared for the following SOT measurements.

Spin transport properties were characterized by anomalous Hall effect (AHE) [25] and SOT measurements, which geometry is schematical illustrated in Fig. 2(a). Figure 2(c) shows the R_H–H loop of anomalous Hall resistance (R_H) variation versus magnetic field for the flexible sample. A direct current I_{dc} = 100 μA was applied along x-direction of the Hall bar device, and a magnetic field (H_z) was applied perpendicular to Hall bar device with a step of 50 Oe. The AHE loop exhibits squareness with a coercivity of about 382 Oe. The SOT induced magnetization switching of the flexible device at as-prepared state was measured under an in-plane field (H_x) of ±300 Oe with a pulse current I = ±11 mA applied along x-direction of the Hall bar device. Figures 2(d) and 2(e) present the R_H variation as a function of the pulse current. The magnetization is switched from $+m_z$ (up) to $-m_z$ (down) under the H_x = +300 Oe when sweeping the pulse current from negative to positive. And the magnetization is switched back to $+m_z$ when sweeping the current

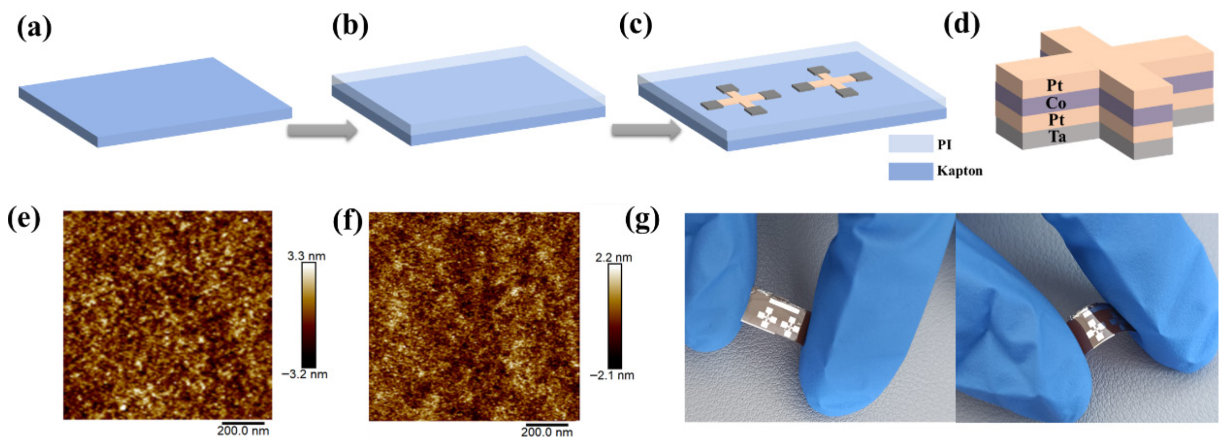

Figure 1 (a)–(c) Schematic diagram of the fabrication process of flexible spintronic devices. (d) The stacking structure of the Hall bar. (e) AFM image of Kapton substrate. (f) AFM image of Kapton/PI surface. (g) Images of the flexible devices at flat and bending states.

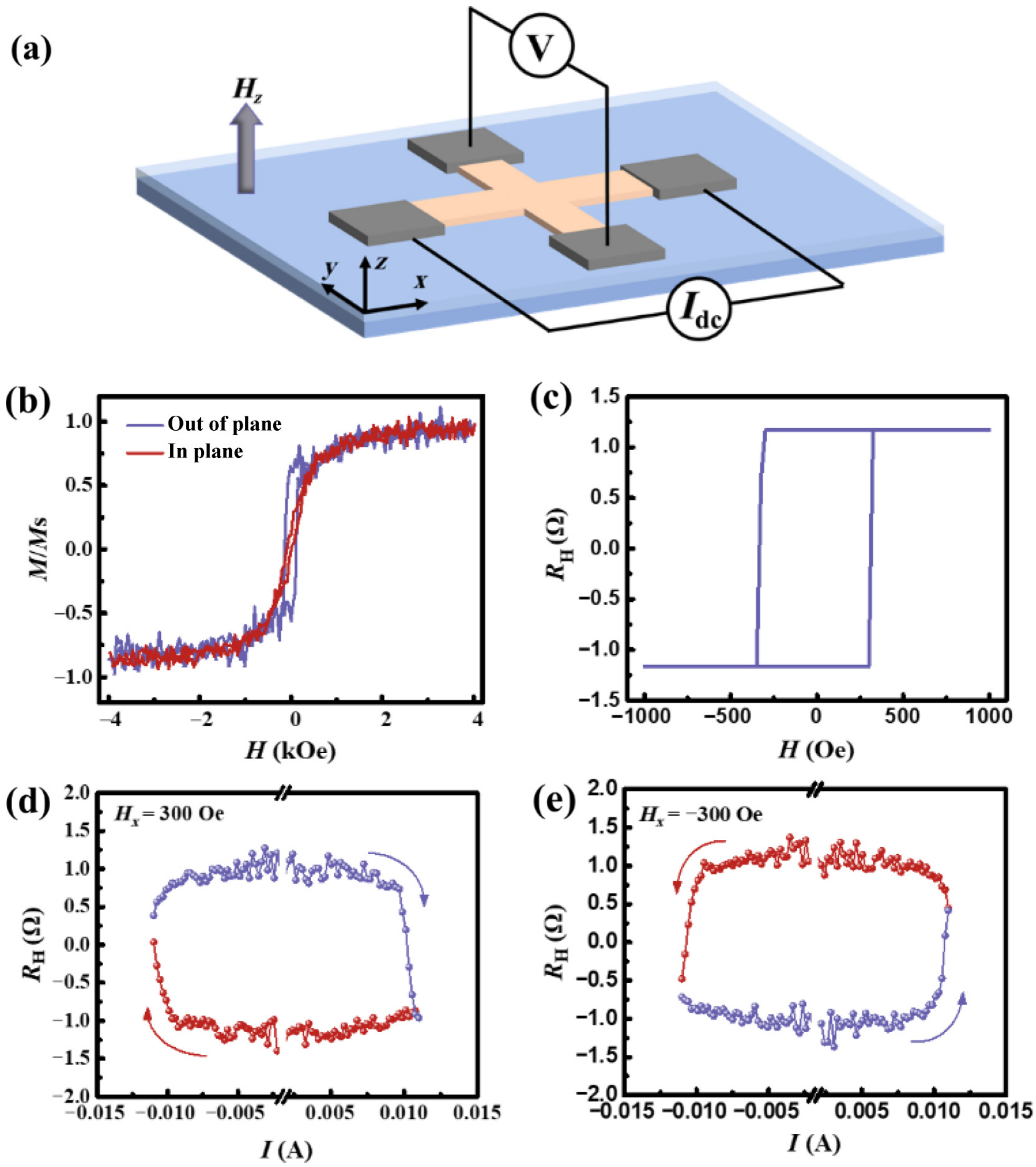

Figure 2 (a) Schematic geometry of the AHE measurement. (b) In-plane and out-of-plane hysteresis loops of the Kapton/PI/Ta (1)/Pt (3)/Co (1.5)/Pt (1) multilayer. (c) The AHE loop of the Kapton/PI/Ta (1)/Pt (3)/Co (1.5)/Pt (1) Hall bar. (d) and (e) The SOT induced magnetization switching loops under the flat condition with an in-plane magnetic field $H_x = \pm 300$ Oe.

from positive to negative. Under the $H_x = -300$ Oe, the opposite switching behavior can be observed. According to the R_H–I loops, J_c is calculated to be about 9.2×10^{10} A·m^{-2}. And the magnetization switching ratio is estimated to be about 98% by using $\Delta R_H/R_H$, where ΔR_H is the change of anomalous Hall resistance. As for the device with a Co layer of 1.0 nm, the magnetization state can also be switched similarly. However, its ΔR_H is insensitive to strain in the following bending state SOT attempts (Fig. S3 in the ESM). This might be explained by the PMA strength of the heterostructures. The orbital moment of the sample with 1.0 nm Co layer is stable in out-of-plane direction due to the strong PMA. However, the orbital moment of the other sample is close to the magnetic anisotropic transition area of the multilayers [26, 27], which can respond to strain easily and lead to effective regulations. This has also been demonstrated in our previous in-plane strain modulated SOT device [21]. Considering the magnetization switching behavior of the device with 1.5 nm Co layer, we fixed the Co layer as 1.5 nm in the following strain modulation measurements.

To understand the process of the SOT induced magnetization switching on the flexible substrate, we tried to directly observe the magnetic domain motion process of the device during magnetization switching by Magnetic Optical Kerr Effect (MOKE) measurements. A perpendicular saturation magnetic field (H_z) was applied to align the magnetic moments along the $-z$ direction before the measurement. Then H_z was removed and an in-plane magnetic field of about ±300 Oe was applied. Next, as schematically illustrated in Fig. 3(a), a pulse current of ±11 mA was applied through the Hall bar to generate SOT, and the nucleation and expansion of domain in the magnetic layer were recorded [28–31], as shown in Figs. 3(b)–3(e). When a pulse current of +11 mA was applied, partial domains of the Hall bar area changed from gray to white, indicating the magnetization switching from $-m_z$ to $+m_z$

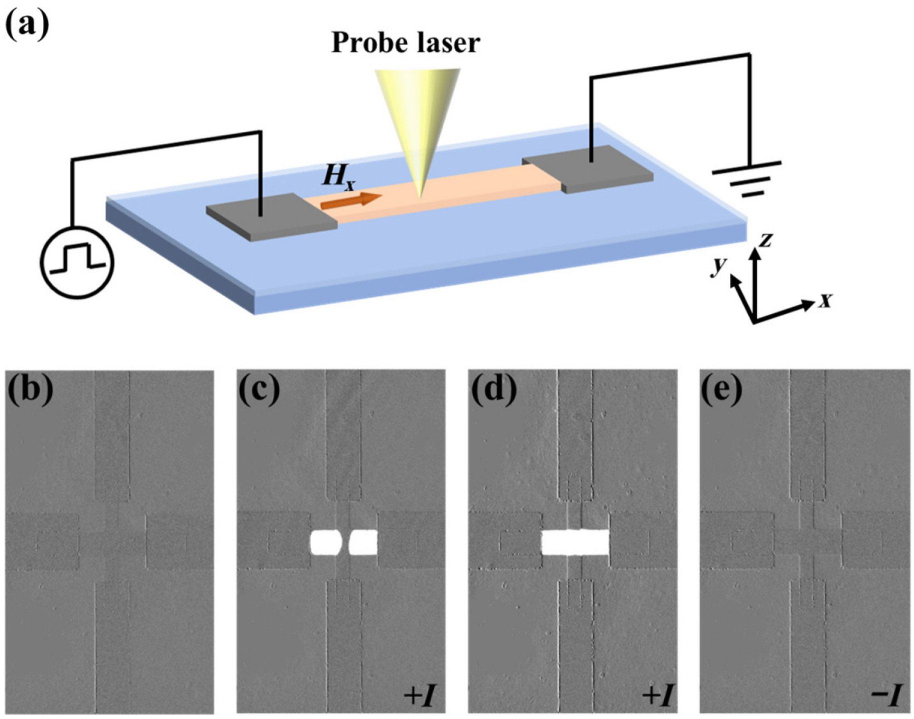

Figure 3 (a) Schematic illustration of the MOKE measurement. (b)–(e) A series of typical MOKE images showing current-induced domain nucleation and expansion process of the Kapton/PI/Ta/Pt/Co/Pt sample by applying a pulse current. The pulse current is set to 11 and −11 mA for (c)–(e), respectively. The gray and white contrasts correspond to the $-m_z$ and $+m_z$ states, respectively.

direction. On applying two more current pulses, the magnetization of the whole Hall bar current channel is switched to $+m_z$ direction. When applied one current pulse of −11 mA, the whole current channel changed to gray, which means the magnetization reversal from the $+m_z$ to $-m_z$ direction, as shown in Fig. 3(e). According to the MOKE images, the magnetization switching ratio of the as-prepared Hall bar is almost 100%. Moreover, MOKE results provide intuitively evidence for the dominant role of the SOT effect in the magnetization switching process [32, 33].

Since the Kapton/PI-based SOT device has been proved to be a desirable candidate for flexible SOT devices, we further studied the bending strain effect on the transport property. The SOT loops of Kapton/PI/Ta/Pt/Co/Pt device were measured under uniaxial tensile bending strain, where the strain direction is illustrated in the inset of Fig. 4(a). The magnitude of the strain can be estimated by $\varepsilon = T/2R$ [34], where R is the curvature radius of the device and T is the total thickness. We use three molds with different curvature radius to get the strain ε approximately as 0.67%, 0.77% and 1.35%, respectively. By using molds, uniform strain can be transferred from the substrate to the thin film, since the thickness of the film is very low in comparison to the substrate. As shown in Fig. 4(a), the multilayer takes on a PMA character based on the results of the R_H–H loops under different strain conditions. The results show that the PMA is enhanced as the strain increases. Similar changes of magnetic anisotropy due to external strain have also been reported previously [20]. These phenomena could be explained by the inverse magnetostriction effect. For the Kapton/PI/Ta/Pt/Co/Pt PMA heterostructure, the tensile strain will enhance the PMA due the negative magnetostriction coefficient of cobalt [10, 35]. Moreover, according to the results of R_H–H loops, H_c increases from 323 to 382 Oe when the tensile strain increases from 0 to 1.35%. The rate of change in H_c is as high as 15%. The values of H_c are extracted from the R_H–H loops under different magnitude of the strain and is presented in Fig. 4(d). It was found that the H_c variation almost takes on a linear trend. Such behavior can be explained as the strength of strain induced anisotropy is significant over the interfacial anisotropy [36, 37]. The R_H–I loops were measured using a pulse current under a magnetic field H_x = ±300 Oe with applying different tensile strain, as presented in Figs. 4(b) and 4(c). The R_H–I loops show obvious change for both J_c and ΔR_H. J_c decreases from 9.2×10^{10} to 8.5×10^{10} A·m^{-2} when the tensile strain increases from 0 to 1.35%. The rate of change in J_c is about 7.6%. The values of J_c are extracted from the R_H–I loops under different magnitude of the strain and is presented in Fig. 4(e). It can be found that the J_c variation almost takes on a linear trend. Such behavior can be explained as follows. J_c is determined by Eq. (1) [21]

$$J_c = \frac{2e}{\hbar}\frac{M_s t_{FM}}{\theta_{SH}}\left(\frac{H_k}{2} - \frac{H_x}{\sqrt{2}}\right) \tag{1}$$

where e is the elementary charge, $\hbar$ denotes the Dirac constant, t_{FM} is the thickness of the Co layer, θ_{SH} is the spin hall angle, M_s is the saturated magnetization, H_x is the external field along the direction of current, and H_k represents the anisotropy field. According to the study of Wong et al. [9], in the Pt/Co system, the spin Hall angle θ_{SH} increases monotonically with tensile strain. Due to the intrinsic properties of non-alloyed metals, the intrinsic scattering contribution in Pt predominates. However, when tensile strain is introduced, the extrinsic contribution from skew scattering increases, leading to an enhancement of θ_{SH}. This conclusion provides a robust explanation for the observed reduction in J_c measured in our experiments. Moreover, as shown in Figs. 4(b) and 4(c), there is also obvious ΔR_H changes between the R_H–I loops measured at different bending states. ΔR_H decreases from 2.23 to 1.81 Ω when the tensile strain increases from 0 to 1.35%. The values of ΔR_H extracted from the R_H–I loops under different magnitude of

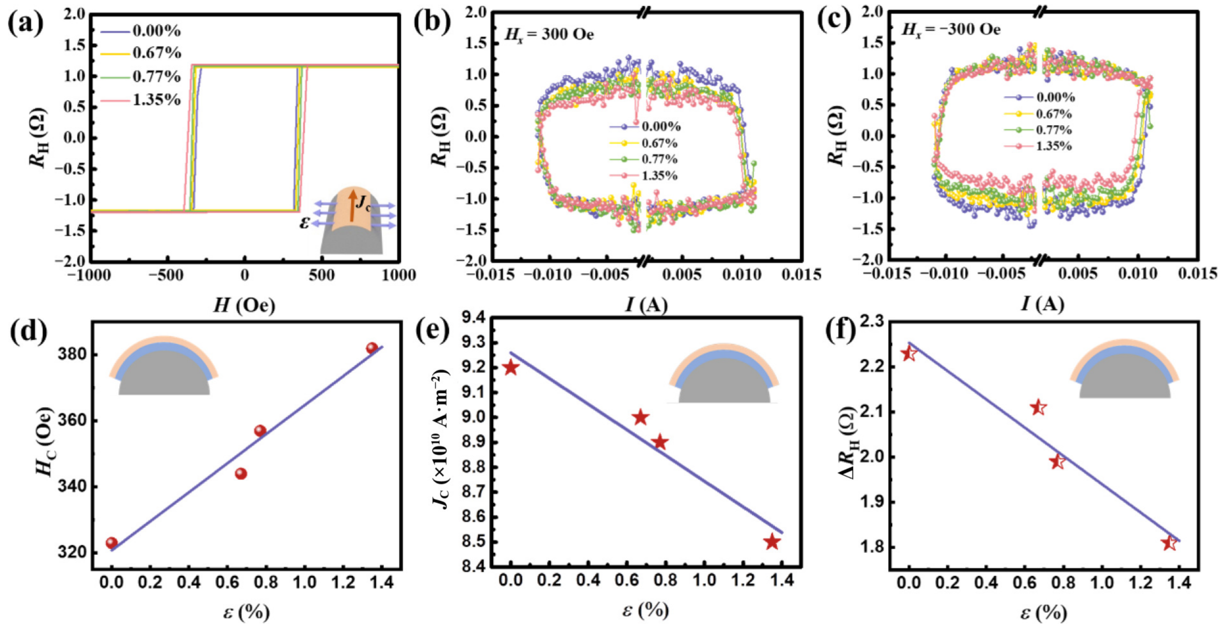

Figure 4 (a) The AHE loops of the Hall bar measured under different strain conditions. (b) and (c) R_H–I loops of the Hall bar measured under different strain conditions and in-plane magnetic fields $H_x = \pm 300$ Oe, respectively. (d)–(f) The variations of H_c, J_c and ΔR_H versus tensile strain.

the strain is presented in Fig. 4(f). According to the fitting results, the ΔR_H also exhibits predominantly linear dependence on the tensile strain. The resistance changes can be explained by domain wall motion. Under the tensile strain state, the propagation of domains is hindered and the growth of domains is prevented, causing the smaller switching ratio under an external magnetic field. Magnetization reversal along with domain nucleation also requires a larger magnetic field under tensile strain due to the increase in overall energy barrier [36]. When the device is back to flat state, the domains are not affected by strain and the required magnetization switching field recovers to the initial value. Consequently, the device achieves fully switching ratio compared to that of the strained state. As a result, the Hall resistance of the device can be controlled by the tensile strain.

Basing on the tensile strain modulation results, we carried out experiments to study the performance of the device serving as SOT-based strain sensors. The Kapton/PI/Ta/Pt/Co/Pt Hall bar device was pasted on finger joint to monitor the action of finger via strain state. Figure 5 shows the operation dependent Hall resistance of the strain sensor, together with the schematic illustrations and images of operations. At each flat and bending state, the Hall resistance was recorded for 20 times and then the magnetization was switched by pulse current under 300 Oe. In each bending cycle, the finger joint was bent to the same angle and then released after holding for 5 s. It can be seen that the Hall resistance is stable at each strain state and is sensitive to the bending action. When the tensile strain increases to 1.35%, ΔR_H decreases by 19%. Moreover, the resistance can be quickly restored to its original value after strain releasing during the repeated bending/releasing cycles. According to the strain response performance, the Kapton/PI-based SOT device is capable of serving as data storage device and strain sensors in flexible applications with low power consumption.

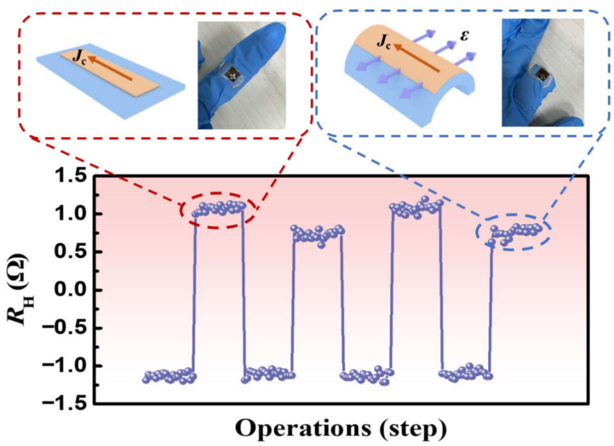

Figure 5 R_H measured by using a read current of 100 μA after the magnetization switching driven by a pulse current of ±11 mA at the flat and 1.35% tensile strain states, together with the schematic illustrations and images of measurements.

3 Conclusions

In this study, we present an effective strain-controlled flexible SOT device on Kapton substrate coated with PI. It is demonstrated that the tensile strain plays an essential role in manipulating the SOT-induced magnetization switching. The coercivity of Pt/Co bilayer can be increased about 15% by a tensile strain of 1.35%. Meanwhile, the J_c decreases about 7.6% under 1.35% tensile strain. The flexible SOT-based device is successfully applied as a strain sensor on finger joint and performs good sensitivity to finger actions. Therefore, the Kapton/PI based device is a kind of promising candidate for power-efficient and flexible spintronics devices through mechanical strain engineering, which will accelerate the development of the flexible data storage devices and strain sensors.

4 Methods

Sample preparation: The PI solution was dropped on Kapton surface and spin coated at 5000 rpm. After spin-coating, the PI film was baked at 200 °C for 5 h on a hot plate followed by annealing at 300 °C for 30 min under normal atmospheric conditions. Then, Ta/Pt/Co/Pt multilayers were deposited by magnetron sputtering at room temperature. The base pressure was better than 1×10^{-5} Pa. During the deposition, the Ar pressure was maintained at 0.5 Pa.

The multilayer was then patterned into Hall bars with dimensions of 10 μm × 20 μm by using standard photolithography and an Ar ion milling technique.

Characterization: The surface roughness of the multilayers was measured by AFM (Bruker, ICON). The magnetic properties of the multilayers were measured using a vibrating sample magnetometer (VSM, Quantum Design, Versalab). MOKE microscope (Magvision Kerr system) was used to observe the process of the magnetization switching. The R_H–H and R_H–I loops were measured in a physical property measurement system (PPMS, Quantum Design, Dyna Cool) by using Keithley 2400 and 2182A systems.

Electronic Supplementary Material: Supplementary material (the characterizations of Kapton/Ta (1 nm)/Pt (3 nm)/Co (t nm)/Pt (1 nm) samples (t = 1.0, 1.5), detailed analysis of M–H loops, and R_H–I loops under different tensile strain states) is available in the online version of this article at https://doi.org/10.26599/NR.2025.94907066.

Data availability

All data needed to support the conclusions in the paper are presented in the manuscript and the Electronic Supplementary Material. Additional data related to this paper may be requested from the corresponding author upon request.

Acknowledgements

This work was partially supported by the National Key R&D Program of China (No. 2022YFA1204004) and National Natural Science Foundation of China (Nos. U24A6001, U23A20548 and 51927802).

Declaration of competing interest

All the contributing authors report no conflict of interests in this work.

Author contributions

M. L. L.: Processed microfabrication, data curation, writing manuscript, experimental design. T. Z. Z. and B. H.: AFM and MOKE measurements, respectively. M. X. W. and J. Q. G.: Revised paper. X. G. X.: Designed and supervised the research. M. L. L., X. G. X., K. K. M., G. Q. Y. and Y. J.: Participated in discussing the results and provided comments and suggestions on the various sections of the manuscript.

Use of AI statement

None.

References

[1] Mannsfeld, S. C. B.; Tee, B. C. K.; Stoltenberg, R. M.; Chen, C. V. H. H.; Barman, S.; Muir, B. V. Q.; Sokolov, A. N.; Reese, C.; Bao, Z. N. Highly sensitive flexible pressure sensors with microstructured rubber dielectric layers. *Nat. Mater.* **2010**, *9*, 859–864.

[2] Lee, S.; Reuveny, A.; Reeder, J.; Lee, S.; Jin, H.; Liu, Q. H.; Yokota, T.; Sekitani, T.; Isoyama, T.; Abe, Y. et al. A transparent bending-insensitive pressure sensor. *Nat. Nanotechnol.* **2016**, *11*, 472–478.

[3] Li, S. B.; Cao, P. J.; Li, F. L.; Asghar, W.; Wu, Y. Z.; Xiao, H. Y.; Liu, Y. W.; Zhou, Y. L.; Yang, H. L.; Zhang, Y. et al. Self-powered stretchable strain sensors for motion monitoring and wireless control. *Nano Energy* **2022**, *92*, 106754.

[4] Zeng, W.; Shu, L.; Li, Q.; Chen, S.; Wang, F.; Tao, X. M. Fiber-based wearable electronics: A review of materials, fabrication, devices, and applications. *Adv. Mater.* **2014**, *26*, 5310–5336.

[5] Kim, J.; Kim, M.; Lee, M. S.; Kim, K.; Ji, S.; Kim, Y. T.; Park, J.; Na, K.; Bae, K. H.; Kyun Kim, H. et al. Wearable smart sensor systems integrated on soft contact lenses for wireless ocular diagnostics. *Nat. Commun.* **2017**, *8*, 14997.

[6] Li, P.; Liu, T.; Chang, H. C.; Kalitsov, A.; Zhang, W.; Csaba, G.; Li, W.; Richardson, D.; DeMann, A.; Rimal, G. et al. Spin-orbit torque-assisted switching in magnetic insulator thin films with perpendicular magnetic anisotropy. *Nat. Commun.* **2016**, *7*, 12688.

[7] Brataas, A.; Kent, A. D.; Ohno, H. Current-induced torques in magnetic materials. *Nat. Mater.* **2012**, *11*, 372–381.

[8] Mihai Miron, I.; Gaudin, G.; Auffret, S.; Rodmacq, B.; Schuhl, A.; Pizzini, S.; Vogel, J.; Gambardella, P. Current-driven spin torque induced by the Rashba effect in a ferromagnetic metal layer. *Nat. Mater.* **2010**, *9*, 230–234.

[9] Hwee Wong, G. D.; Xu, Z.; Gan, W. L.; Ang, C. C. I.; Law, W. C.; Tang, J. X.; Zhang, W.; Wong, P. K. J.; Yu, X. J.; Xu, F. et al. Strain-mediated spin-orbit torque enhancement in Pt/Co on flexible substrate. *ACS Nano* **2021**, *15*, 8319–8327.

[10] Zhao, S. S.; Zhou, Z. Y.; Li, C. L.; Peng, B.; Hu, Z. Q.; Liu, M. Low-voltage control of $(Co/Pt)_x$ perpendicular magnetic anisotropy heterostructure for flexible spintronics. *ACS Nano* **2018**, *12*, 7167–7173.

[11] Lee, O.; You, L.; Jang, J.; Subramanian, V.; Salahuddin, S. Flexible spin-orbit torque devices. *Appl. Phys. Lett.* **2015**, *107*, 252401.

[12] Li, M. L.; Li, C. X.; Xu, X. G.; Wang, M. X.; Zhu, Z. Q.; Meng, K. K.; He, B.; Yu, G. Q.; Hu, Y. F.; Peng, L. M. et al. An ultrathin flexible programmable spin logic device based on spin-orbit torque. *Nano Lett.* **2023**, *23*, 3818–3825.

[13] Farle, M.; Platow, W.; Anisimov, A. N.; Poulopoulos, P.; Baberschke, K. Anomalous reorientation phase transition of the magnetization in fct Ni/Cu(001). *Phys. Rev. B* **1997**, *56*, 5100–5103.

[14] Baek, S. H. C.; Park, K. W.; Kil, D. S.; Jang, Y.; Park, J.; Lee, K. J.; Park, B. G. Complementary logic operation based on electric-field controlled spin-orbit torques. *Nat. Electron.* **2018**, *1*, 398–403.

[15] Luo, Z. C.; Hrabec, A.; Dao, T. P.; Sala, G.; Finizio, S.; Feng, J. X.; Mayr, S.; Raabe, J.; Gambardella, P.; Heyderman, L. J. Current-driven magnetic domain-wall logic. *Nature* **2020**, *579*, 214–218.

[16] Zhao, X. N.; Dong, Y. N.; Chen, W. B.; Xie, X. J.; Bai, L. H.; Chen, Y. X.; Kang, S. S.; Yan, S. S.; Tian, Y. F. Purely electrical controllable complete spin logic in a single magnetic heterojunction. *Adv. Funct. Mater.* **2021**, *31*, 2105359.

[17] Wan, C. H.; Zhang, X.; Yuan, Z. H.; Fang, C.; Kong, W. J.; Zhang, Q. T.; Wu, H.; Khan, U.; Han, X. F. Programmable spin logic based on spin hall effect in a single device. *Adv. Electron. Mater.* **2017**, *3*, 1600282.

[18] Zhang, Y. L.; Liu, J.; Dong, Y. Q.; Wu, S. Z.; Zhang, J. Y.; Wang, J.; Lu, J. D.; Rückriegel, A.; Wang, H. C.; Duine, R. et al. Strain-driven dzyaloshinskii-moriya interaction for room-temperature magnetic skyrmions. *Phys. Rev. Lett.* **2021**, *127*, 117204.

[19] Okabayashi, J.; Usami, T.; Mahfudh Yatmeidhy, A.; Murakami, Y.; Shiratsuchi, Y.; Nakatani, R.; Gohda, Y.; Hamaya, K. Strain-driven dzyaloshinskii-moriya interaction for room-temperature magnetic skyrmions. *NPG Asia Mater.* **2024**, *16*, 3.

[20] Matsumoto, H.; Ota, S.; Koyama, T.; Chiba, D. Control of magnetic anisotropy in a Co thin film on a flexible substrate by applying biaxial tensile strain. *Appl. Phys. Lett.* **2021**, *118*, 022406.

[21] Wang, M. X.; Guo, Q.; Xu, X. G.; Zhang, Z. Y.; Ren, Z. Y.; Zhu, L. B.; Meng, K. K.; Chen, J. K.; Wu, Y.; Miao, J. et al. Lateral electric-

field-controlled perpendicular magnetic anisotropy and current-induced magnetization switching in multiferroic heterostructures. *Adv. Electron. Mater.* **2020**, *6*, 2000229.
[22] Carcia, P. F. Perpendicular magnetic anisotropy in Pd/Co and Pt/Co thin-film layered structures. *J. Appl. Phys.* **1988**, *63*, 5066–5073.
[23] Xie, Q. D.; Lin, W. N.; Yang, B. S.; Shu, X. Y.; Chen, S. H.; Liu, L.; Yu, X. J.; Breese, M. B. H.; Zhou, T. J.; Yang, M. et al. Giant enhancements of perpendicular magnetic anisotropy and spin-orbit torque by a MoS_2 layer. *Adv. Mater.* **2019**, *31*, 1900776.
[24] Grimsditch, M.; Jaccard, Y.; Schuller, I. K. Magnetic anisotropies in dot arrays: Shape anisotropy versus coupling. *Phys. Rev. B* **1998**, *58*, 11539–11543.
[25] Hu, J. F.; Ernst, B.; Tu, S.; Kuveždić, M.; Hamzić, A.; Tafra, E.; Basletić, M.; Zhang, Y. G.; Markou, A.; Felser, C. et al. Anomalous hall and Nernst effects in Co_2TiSn and $Co_2Ti_{0.6}V_{0.4}Sn$ Heusler thin films. *Phys. Rev. Appl.* **2018**, *10*, 044037.
[26] Yang, Q.; Nan, T. X.; Zhang, Y. J.; Zhou, Z. Y.; Peng, B.; Ren, W.; Ye, Z. G.; Sun, N. X.; Liu, M. Voltage control of perpendicular magnetic anisotropy in multiferroic $(Co/Pt)_3/PbMg_{1/3}Nb_{2/3}O_3–PbTiO_3$ heterostructures. *Phys. Rev. Appl.* **2017**, *8*, 044006.
[27] Nakajima, N.; Koide, T.; Shidara, T.; Miyauchi, H.; Fukutani, H.; Fujimori, A.; Iio, K.; Katayama, T.; Nývlt, M.; Suzuki, Y. Perpendicular magnetic anisotropy caused by interfacial hybridization via enhanced orbital moment in Co/Pt multilayers: Magnetic circular X-ray dichroism study. *Phys. Rev. Lett.* **1998**, *81*, 5229–5232.
[28] Cao, J. W.; Chen, Y. F.; Jin, T. L.; Gan, W. L.; Wang, Y.; Zheng, Y. Q.; Lv, H.; Cardoso, S.; Wei, D.; Lew, W. S. Spin orbit torques induced magnetization reversal through asymmetric domain wall propagation in Ta/CoFeB/MgO structures. *Sci. Rep.* **2018**, *8*, 1355.
[29] Ma, Q. L.; Li, Y. F.; Gopman, D. B.; Kabanov, Y. P.; Shull, R. D.; Chien, C. L. Switching a perpendicular ferromagnetic layer by competing spin currents. *Phys. Rev. Lett.* **2018**, *120*, 117703.
[30] Vélez, S.; Schaab, J.; Wörnle, M. S.; Müller, M.; Gradauskaite, E.; Welter, P.; Gutgsell, C.; Nistor, C.; Degen, C. L.; Trassin, M. et al. High-speed domain wall racetracks in a magnetic insulator. *Nat. Commun.* **2019**, *10*, 4750.
[31] Emori, S.; Bauer, U.; Ahn, S. M.; Martinez, E.; Beach, G. S. D. Current-driven dynamics of chiral ferromagnetic domain walls. *Nat. Mater.* **2013**, *12*, 611–616.
[32] Zhang, R. Q.; Liao, L. Y.; Chen, X. Z.; Xu, T.; Cai, L.; Guo, M. H.; Bai, H.; Sun, L.; Xue, F. H.; Su, J. et al. Current-induced magnetization switching in a CoTb amorphous single layer. *Phys. Rev. B* **2020**, *101*, 214418.
[33] Xie, X. J.; Zhao, X. N.; Dong, Y. N.; Qu, X. L.; Zheng, K.; Han, X. D.; Han, X.; Fan, Y. B.; Bai, L. H.; Chen, Y. X. et al. Controllable field-free switching of perpendicular magnetization through bulk spin-orbit torque in symmetry-broken ferromagnetic films. *Nat. Commun.* **2021**, *12*, 2473.
[34] Liu, E.; Fache, T.; Cespedes-Berrocal, D.; Zhang, Z.; Petit-Watelot, S.; Mangin, S.; Xu, F.; Rojas-Sánchez, J. C. Strain-enhanced charge-to-spin conversion in Ta/Fe/Pt multilayers grown on flexible mica substrate. *Phys. Rev. Appl.* **2019**, *12*, 044074.
[35] Kwon, J. H.; Kwak, W. Y.; Cho, B. K. Magnetization manipulation of a flexible magnetic sensor by controlled stress application. *Sci. Rep.* **2018**, *8*, 15765.
[36] Pandey, E.; Singh, B. B.; Sharangi, P.; Bedanta, S. Strain engineered domain structure and their relaxation in perpendicularly magnetized Co/Pt deposited on flexible polyimide. *Nano Express* **2020**, *1*, 010037.
[37] Ota, S.; Hibino, Y.; Bang, D.; Awano, H.; Kozeki, T.; Akamine, H.; Fujii, T.; Namazu, T.; Takenobu, T.; Koyama, T. et al. Strain-induced reversible modulation of the magnetic anisotropy in perpendicularly magnetized metals deposited on a flexible substrate. *Appl. Phys. Express* **2016**, *9*, 043004.